UNIVERSITY OF LATVIA

Summary of Doctoral Thesis

Abdelqader Zaben

DYNAMICS OF SPONTANEOUSLY MAGNETIZED MICRO-FILAMENTS UNDER AN EXTERNAL MAGNETIC FIELD: EXPERIMENTAL INVESTIGATION

Riga 2022

UNIVERSITY
OF LATVIA

FACULTY OF PHYSICS, MATHEMATICS AND OPTOMETRY

Abdelqader Zaben

DYNAMICS OF SPONTANEOUSLY MAGNETIZED MICRO-FILAMENTS UNDER AN EXTERNAL MAGNETIC FIELD: EXPERIMENTAL INVESTIGATION

SUMMARY OF DOCTORAL THESIS

Submitted for the Doctoral degree in Physics
Subfield: Fluid and gas mechanics

Riga, 2022

The doctoral thesis was carried out at the Chair of Theoretical Physics, Department of Physics, Faculty of Physics, Mathematics and Optometry, University of Latvia, from 2018 to 2022.

The thesis contains the introduction, 4 chapters, reference list, 2 appendices.
Form of the thesis: Dissertation.

Supervisors: Prof. **Andrejs Cēbers** and *Dr.* **Guntars Kitenbergs**.

Reviewers:

1) *Dr. phys.* **Juris Prikulis**, Senior researcher,
   Institute of Chemical Physics, University of Latvia;
2) *Dr.* **Peter Kopčanský**, Professor,
   Institute of Experimental Physics, Slovak Academy of Sciences, Slovakia;
3) *Dr.* **Mojca Vilfan**, Research Associate,
   Jožef Stefan Institute, Slovenia.

The thesis will be defended at the public session of the Promotion Council of Physics and Astronomy of the University of Latvia on December 2nd, 2022, at 15:30 in the Auditorium _____ of the House of Science, University of Latvia, Jelgavas street 3, in Riga, Latvia.

The full text of thesis and its summaries are available at the Library of the University of Latvia (Kalpaka blvd. 4, Riga, Latvia) and at the University of Latvia Academic Library (Rupniecibas str. 10, Riga, Latvia).

Chairman of the Specialized Promotion Council
of the scientific section of the Physics and
Astronomy at the University of Latvia — *Dr. phys.* **Andris Jakovičs**

Secretary of the Specialized
Promotion Council — **Sintija Siliņa**

ISBN 978-9934-18-894-7
ISBN 978-9934-18-895-4 (PDF)

Annotation

Micro-devices manipulated by an external force is an interesting topic of research in terms of potential applications, as for mixing in microfluidics and targeted cargo delivery in bio-medical applications. Magnetically actuated robots, as investigated here, gives the advantage of both having on-demand motion control and safe bio-compatibility. In this work, the dynamics of magnetic filaments is investigated experimentally under both rotating and pulsed magnetic field. The filaments are made from ferromagnetic particles linked together by deoxyribonucleic acid (DNA) fragments. The experiments were conducted under operating different conditions which allowed adequate comparison with numerical simulations results, identifies limitations in models developed in previous studies and gives a preliminary insight for using ferromagnetic filaments for mixing and as cargo delivery applications.

Contents

1 Introduction **5**
1.1 Research actuality and literature review 5
1.2 Objective and research questions 7
1.3 Experimental methods 8
1.4 Approbation of the results 10
1.4.1 List of scientific publications related to the thesis . . 10
1.4.2 List of scientific seminars and conferences 11
1.4.3 Research project 12
1.5 Author's previous education and scientific experience . . . 12

2 Filament dynamics under a rotating field **13**

3 Filament dynamics under pulsed field **19**

4 Local flow measurements **26**

5 Summary and conclusions **31**
5.1 Thesis 31

References **32**

1 Introduction

1.1 Research actuality and literature review

Research on magnetically actuated micro-robots has become a topic of increasing interest in the past ten years (Koleoso et al. 2020), due to their potential applications, as for example, mixing (Biswal and Gast 2004; Chen and Zhang 2017; Shanko et al. 2019), targeted cargo delivery (Nguyen et al. 2021; Ahmed et al. 2017) and microrheology (Brasovs et al. 2015). Hence, understanding the dynamics of such devices in their operating environment became crucial from the point of view of feasibility, design and development. Self-propelling microdevices working in the realm of low Reynolds numbers is challenging object for research, since viscous forces exerted by the fluid dominate over inertial forces. When the inertia effects are negligible, the flow regime is reversible, as first experimentally realized by Taylor 1967. Purcell 1977, in his well known paper, *Life at low Reynolds number*, formulated 'the scallop theorem' addressing the issue of this reversibility on reciprocal motion to achieve propulsion and the way to overcome it by having more than one degree of freedom. Similarly for mixing in microfluidics, where momentum transfer is mainly dependent on molecular diffusion, local mixing is becoming important to enable lab on chip devices (Drew et al. 2016), considering the constraints of space and time for diffusion to take place. Such important potential applications in the field of biomedicine and microfluidics give the motivation to conduct this study.

One design of devices actuated by external magnetic field, that have been commonly used in research, are chains consisting of connected micron size magnetic particles. This design gives the advantage of easy in-house manufacturing at a lab, as well as the flexibility to explore the dynamics of various configurations for preliminary studies. For example, as first published investigations for applications, chain of 1 μm paramagnetic particles, driven by oscillating transverse magnetic field (Dreyfus et al. 2005), was used to investigate the swimming behaviour with an added cargo.

Moreover, chains made from 1.4 μm para-magnetic particles, propelled by a rotating magnetic field, were used to study the dynamics for mixing application (Biswal and Gast 2004).

The dynamics of flexible magnetic filaments is interesting since their behaviour are governed by both magnetic and elastic forces. Under the action of static field applied in one dimension, paramagnetic filaments were found to either align with the magnetic field direction or deform having and S-like or U-like shape, as experimentally observed by Goubault et al. 2003. Under the action of rotating field profile in a plane, the filament experiences a torque of magnetic origin which is opposed by hydrodynamic friction force as the result of the filament rotation (Spatafora-Salazar et al. 2021). At relatively low frequencies, for a filament made from super-paramagnetic particles different rotational modes were observed experimentally, namely rigid, wagging (S-like shapes) and folding. The mode of rotation depends on the filament flexibility, while the filament may rotate synchronously or asynchronously with the magnetic field (Kuei et al. 2017).

A theory that was adopted by several authors to model flexible magnetic filaments are based on the modified Kirchhoff rod theory to account for magnetic energy (Cēbers 2003; Barreto et al. 2022). The force and torque acting in the cross section of the rod are derived by energy variation which includes the elastic bending energy and energy of magnetic rod in an applied field (Cēbers 2003). In the case of ferromagnetic material, the magnetic moment per unit length of the rod $\vec{M}$ is antiparallel the local tangent direction $\vec{t}$: $\vec{M} = -M\vec{t}$. The torque balance reads (Ērglis et al. 2010),

$$\frac{d\vec{K}}{dl} + \vec{t} \times \vec{F} - M\vec{t} \times \vec{H} = 0 \tag{1}$$

and the magnetic force gives $\vec{F}_m = M\vec{H}$. The balance of the viscous, elastic and magnetic forces reads

$$\vec{\vec{\zeta}} \frac{\partial \vec{r}}{\partial t} = -A_b \frac{\partial^4 \vec{r}}{\partial l^4} + \frac{\partial (\Lambda \vec{t})}{\partial l} \tag{2}$$

where $\vec{\vec{\zeta}}_{ik} = \zeta_\perp \delta_{ik} + (\zeta_\parallel - \zeta_\perp) t_i t_k$ is the matrix of hydrodynamic drag coefficients, Λ is the tension to sustain the inextensibility of the rod and A_b is the bending modulus.

The length is scaled with the length of the filament L, time with the elastic relaxation time $\tau = \zeta_\perp L^4 / A_b$, the elastic force by A_b / L^2. As a result behavior of the rod is determined by the magnetoelastic number $Cm = MHL^2/A_b$ and $\omega\tau$, where ω is the characteristic frequency of the AC field.

1.2 Objective and research questions

The main **aim** of this thesis is to experimentally investigate the dynamics of semi-flexible magnetic chains, made of ferromagnetic particles linked by elastic polymers, under various magnetic field profiles. This work is proposed to fill research gaps in the literature available in the public domain, where the focus in this field is mainly oriented in using para-magnetic particles, by trying to answer the following **questions**,

- How do the filaments behave under a rotating magnetic field? When sweeping through field frequencies, can one observe a change in the behavior of the filament with a characteristic critical frequency?

- Can a ferromagnetic filament propel under a periodic field inversion profile, as numerically proposed by Belovs and Cēbers 2009?

- What are the flow characteristics around the filaments under a rotating magnetic field?

In this summary, a brief description of the methods is presented in Section 1.3. The filament dynamics under a rotating magnetic field is presented in Chapter 2. In Chapter 3 and 4 the filament behaviour under pulsed field and velocity measurements is presented respectively. Finally, this work conclusions are presented in Chapter 5.

1.3 Experimental methods

Throughout this work, the method used to form filaments was adapted from the work done by K. Ērglis 2010. The filament is formed by linking magnetic particles with DNA fragments. The ferro-magnetic particles used are supplied by Spherotech, with the mean diameters of 4.21 μm and 4.39 μm for the lots used. These particles are made of polystyrene, which is coated with a thin layer of chromium oxide and afterwards functionalized with streptavidin. The deoxyribonucleic acid (DNA) fragments are supplied by the Latvian Biomedical Research and Study Centre, which are 1000 base pair (bp) long and biotinylated on both their ends.

The procedures adopted as follows,

- First, 10 μL DNA fragment solution (182 ± 10 μg/ml) is mixed with 2 ± 0.5 μL magnetic particles (1% w/v) and 0.5 ml 10 % TE buffer solution (made by mixing 7.5 pH TE buffer solution with distilled water) in 1.5 - 2 ml test tubes.

- The test tube is then placed between two strong permanent magnets, made from a Neodymium alloy. Dimensions of each magnet are $5 \times 5 \times 1$ cm. Magnets are fixed at 7 cm apart and can provide a homogeneous field of ≈ 500 Oe.

The experimental setup shown in Fig.1 consists of; in-house built coil system, which has 6 coils to generate magnetic field in the three dimensions. The coils are connected to AC power supplies (Kepco BOP 20-10M), The coil system is capable of producing a maximum magnetic field of 51 Oe. The desired field profile is generated by a Labview code sent to the power supplies through National Instruments data acquisition card (NI PCI-6229). The images were acquired by Basler ac1920-155um camera, which can deliver up to 200 frames per second. The camera is synchronized with the system either by receiving a pulsed digital input signal through the DAQ cards or output signal for registering the current readings. For sample observation, an optical (Leica DMI3000B) microscope was used, under either 40× and 10× magnification in bright field mode.

The fluidic cells are made by using two microscope glass slides separated by 211 μm double-sided adhesive tape, that have a maximum volume capacity of $\approx$ 20 μl.

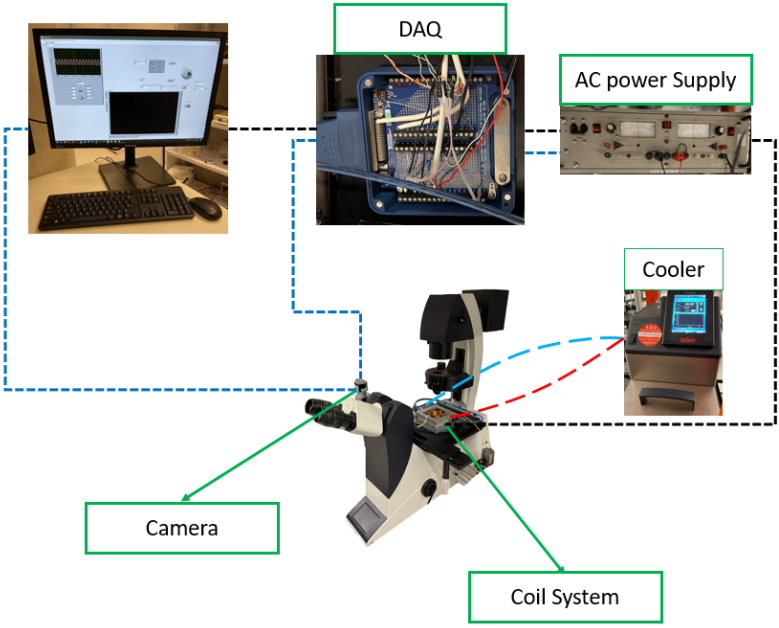

Figure 1: Experimental setup

The micro-Particle Image Velocimetry (μ-PIV) setup used for velocity measurements is provided by Dantec Dynamics, Fig.2, consists of; HiSense MkII camera which has a CCD sensor with maximum frame rate 12.2 Hz and a minimum interframe time 200 ns in double frame mode. A double pulsed laser ($\lambda = 532$ nm) which is used as a light source for exciting the tracer particles, with a maximum frequency of 50 Hz. The camera and the laser are synchronized through a timer box (NI PCI-6602). The filament samples are observed by an inverted optical microscope (Leica DMIL), under Y3 filter cube and 40x objective.

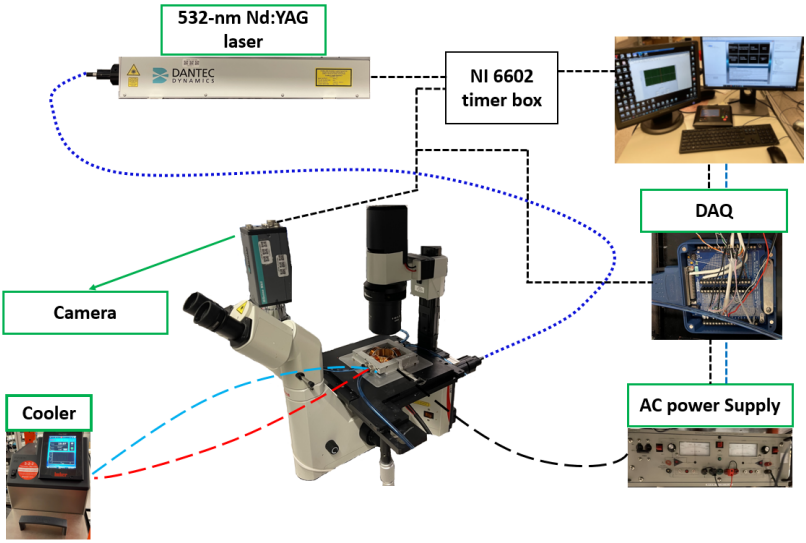

Figure 2: Experimental setup for velocity measurements

1.4 Approbation of the results

1.4.1 List of scientific publications related to the thesis

- A. Zaben, G. Kitenbergs, A. Cēbers (2021) Instability caused swimming of ferromagnetic filaments in pulsed field. Scientific Reports, 11, 23399.

- A. Zaben, G. Kitenbergs, A. Cēbers (2020) 3D motion of flexible ferromagnetic filaments under rotating magnetic field. Soft Matter, 16, 4477-4483.

- A. Zaben, G. Kitenbergs, A. Cēbers (2020) Deformation of flexible ferromagnetic filaments under a rotating magnetic field. Journal of Magnetism and Magnetic Materials, 499, 166233.

1.4.2 List of scientific seminars and conferences

- A.Zaben, A.Cēbers, G.Kitenbergs. Deformation of flexible ferromagnetic filaments under rotating field. Magnetic Soft Matter, 77th International Conference of the University of Latvia, February 1, 2019, Riga.

- A.Zaben, G.Kitenbergs, A.Cēbers. Deformation of flexible ferromagnetic filaments under a rotating magnetic field. International Conference on Magnetic Fluids, July 8-12,2019, Paris, France.

- A.Zaben, G.Kitenbergs, A.Cēbers. Flexible ferromagnetic filaments as micro-mixers. Magnetic Soft Matter, 78th International Conference of the University of Latvia, February 14, 2020, , Riga.

- A.Cēbers, A.Zaben, G.Kitenbergs. Ferromagnetic swimmers: experiment, theory and simulation. Magnetic Soft Matter. 79th International Conference of the University of Latvia, February 11, 2021, Riga.

- A.Zaben, G.Kitenbergs, A.Cēbers. Movement diversity of flexible ferromagnetic filaments - from rotation to propulsion. Priority research topic "Nano, Quantum Technologies, and Innovative Materials". 79th International Conference of the University of Latvia, February 15, 2021, Riga.

- A.Zaben, A.Cēbers, G.Kitenbergs, Rotation and swimming of flexible ferromagnetic filaments, Latvian-Brazilian meeting on Active and Soft Matter Physics, 80th International Conference of the University of Latvia, February 3, 2022, Riga.

- A.Cebers, A.Zaben, G.Kitenbergs, M.Belovs. Magnetic filaments: shapes, stability and self-propulsion. APS March Meeting 2022, March 14-18, 2022, Chicago, USA.

1.4.3 Research project

The work done here is associated with *"Magnetics and Microhydrodynamics"* innovative training network project, funded by the European Union's Horizon 2020 research and innovation programme under grant agreement No. 766007.

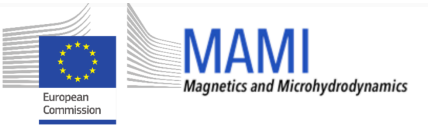

1.5 Author's previous education and scientific experience

Education

- MSc Fluid Mechanics and Energetics, Grenoble INP, Grenoble, France, 2017.
- MSc Thermal Power (Gas turbine technology option), Cranfield University, UK, 2014.
- BEng Aerospace and Aeronautical Engineering, University of Leeds, UK, 2011.

Scientific experience

- Research stay, Max Planck Institute for Dynamics and Self-Organizations (MPIDS), Göttingen, Germany. 'Investigation of flow field around *Chlamydomonas reinhardtii* in confined spaces'
- Internship, Institute of Physics of Rennes. Rennes, France. 'Investigation of the training history on the properties of dense suspensions.'

2 Filament dynamics under a rotating field

The behaviour of the filaments is investigated under the action of a rotating magnetic field. The filament under this field profile was found to undergo two regimes, where transition is at a characteristic critical frequency f_c: a 2D in-plane rotation at lower frequencies and a 3D motion for higher frequencies. The experiments where conducted using filaments with different length L, at a range of frequencies f and field strength H. An example of deformed filament shapes observed is shown in Fig.3. In images (a)-(c) the difference of deformed shapes of a filament with $L = 41$ μm can be seen

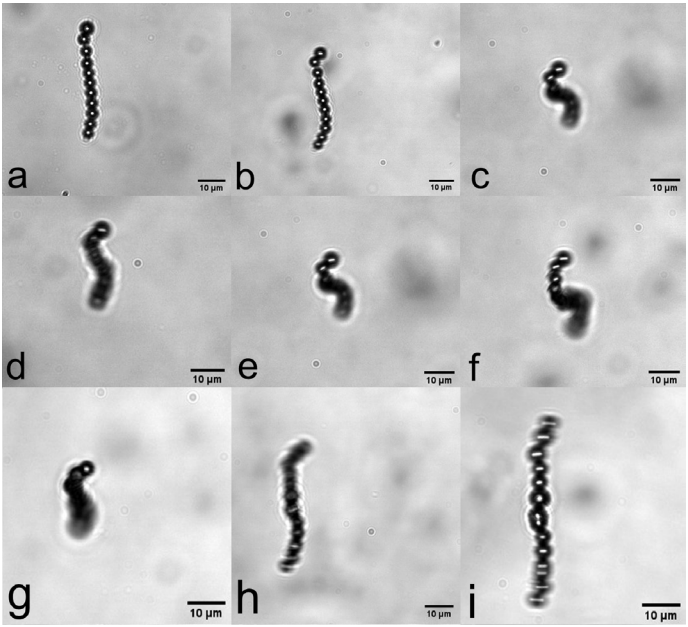

Figure 3: Shapes of deformed filaments under rotating magnetic field. Filament with $L = 41$ μm at $H = 17.2$ Oe for frequencies (a) $f = 1$ Hz, (b) $f = 4$ Hz, (c) $f = 9$ Hz. Filaments at $H = 17.2$ Oe and $f = 8$ Hz for filaments with lengths (d) $L = 33$ μm, (e) $L = 41$ μm, (f) $L = 65$ μm. Filament with $L = 46$ μm at $f = 5$ Hz and magnetic fields (g) $H = 4.3$ Oe, (h) $H = 12.9$ Oe, (i) $H = 25.8$ Oe.

for an increasing frequency at a constant field strength H. In Fig.3(a) & (b) it is visible that the filament performs a steady in-plane rotation with a slight 'S'-like deformation. While in Fig.3(c), the filament undergoes a 3D motion, observable experimentally due to the blurred filament body shape when focusing on one of the filament tips. For longer filaments at the same constant frequency above f_c and the same field strength, higher deformations are observed. This can be seen in Fig.3(d), (e) and (f), where $L = 33$ μm, $L = 41$ μm and $L = 65$ μm respectively. Similarly, the observed shapes of a filament with length $L = 46$ μm are shown in Fig.3(g)-(i) for a frequency $f = 5$ Hz when increasing the field strength.

For filament rotations below critical frequency, the filament dynamics here is characterized by measuring the angle between the magnetic field direction and the tangent angle at the filament centre ϑ. The angle ϑ was calculated for filaments with three different lengths L for a range of frequencies and field strengths. The results obtained showing the effect of

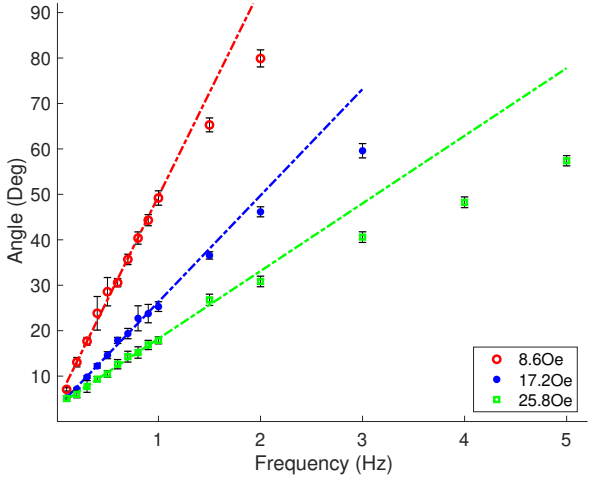

Figure 4: Relationship between the angle ϑ and frequency f, under rotating magnetic field with different strengths, $H = 8.6$ Oe (red), $H = 17.2$ Oe (blue) and $H = 25.8$ Oe (green) for a filament with a length $L = 46.3$ μm.

varying the magnetic field strength under a range of frequencies (0.1 Hz to 5 Hz) for the same filament with a length $L = 46.3$ μm is shown in Fig.4. The circles, points and squares donate the calculated values of ϑ at three magnetic fields 8.6 Oe, 17.2 Oe and 25.5 Oe respectively. From the results in Fig.4 it is visible that the increase of the magnetic field strength results in a lower angle ϑ. To approximate the filament magnetization from the obtained experimental results, relation (3) obtained theoretically by considering rigid rod is used, where ζ is the hydrodynamic coefficient approximated by $4\pi\eta$, the viscosity of the fluid η is approximated with the water viscosity 0.01 P and the constant a in $\frac{\theta}{f} = a\,\frac{1}{H}$ was found experimentally to be 6.8 Oe·s,

$$\vartheta = 0.086\frac{\omega\tau}{Cm} \tag{3}$$

The filament bending modulus is measured by registering the displacement of a filament tip along the y axis over time after rotating field is switched off. The measured y-displacement over time is shown in Fig.5 and was found to have an exponential dependence for three filaments with different lengths. The decrements of the filament relaxation from the decay

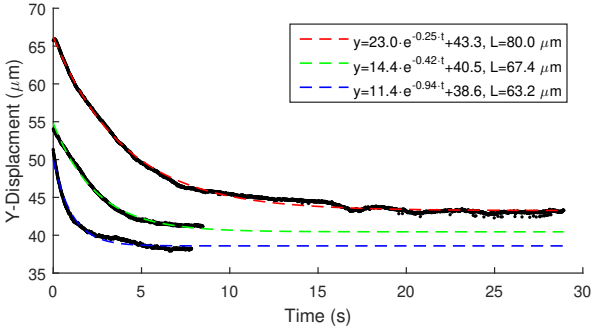

Figure 5: Filament relaxation behaviour for different filament lengths L and the initial rotating field conditions: $L = 80.0$ μm, $f = 1.0$ Hz and $H = 8.6$ Oe (red curve). $L = 63.2$ μm, $f = 1.0$ Hz and $H = 13.7$ Oe (blue curve). $L = 67.4$ μm, $f = 1.5$ Hz and $H = 8.6$ Oe (green curve).

rate were found to be 0.25 s^{-1}, 0.42 s^{-1} and 0.25 s^{-1} for filaments with length $L = 80$ μm, 76.4 μm and 63.2 μm respectively. Using the solution for a free rod with the unclamped boundary conditions for the elastic micro filament problem (eq: 4), as presented by Wiggins et al. 1998, the bending modulus A_b is then estimated using the decay rates $1/\tau$ obtained from the experimental data, where the estimated value is $A_b = 6.5 \pm 3.4 \cdot 10^{-13}$.

$$\frac{1}{\tau} = 3.93^4 L^{-4} A_b/\zeta \tag{4}$$

We characterize the filament deformations as the ratio $\frac{R}{L}$ between the radius of the tip trajectory R with the filament length L. The experimental results obtained for the relationship between R/L and frequency are shown in Fig.6 for filaments with three different lengths. Red, green and blue diamonds denote data points for L = 65 μm, 41 μm and 33 μm respectively measured under a constant field strength $H = 17.2$ Oe. This relationship shows that an increase in frequency first results in a minor decrease of R/L, which is followed by an abrupt drop of R/L, which can be seen clearly for

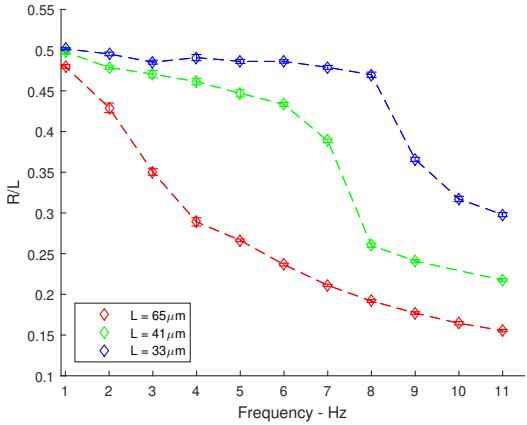

Figure 6: Experimental data for the relationship between R/L and frequency f. Deformation of filaments with different length is measured operating at the field strength $H = 17.2$ Oe.

$L = 41$ μm and 33 μm data behaviour in Fig.6. This abrupt change was observed experimentally to occur during the transition from a 2D planar regime to 3D motion for frequencies above the critical frequency f_c. A further increase in the frequency was observed to have lower influence on R/L. Moreover, longer filaments were found to have lower values of critical frequency f_c.

From the results obtained, it can be seen that flexible chains formed by linked ferromagnetic particles, under the action of a 2D rotating magnetic field, rotates synchronously with the magnetic field in its plane of rotation or undergo a transition to a 3D motion. This transition to a 3D rotating motion was previously predicted numerically for magnetic particles in a rotating field (Cīmurs and Cēbers 2013) and where experimentally realized in a recent study for nano-rods made from ferro-magnetic material (Palkar et al. 2019). Moreover, their behaviour differs from chains made by linking paramagnetic particles, which undergo an in-plane back and forth motion rotations at frequencies above critical (Frka-Petesic et al. 2011). Numerical simulations were made using the model presented in chapter 1, with the addition of small perturbations which the system may experience. The results obtained for R/L dependence on frequency in comparison with experimental data shows good agreement, as shown in Fig.7, for filament with $L = 46$ μm operating at different field strength H.

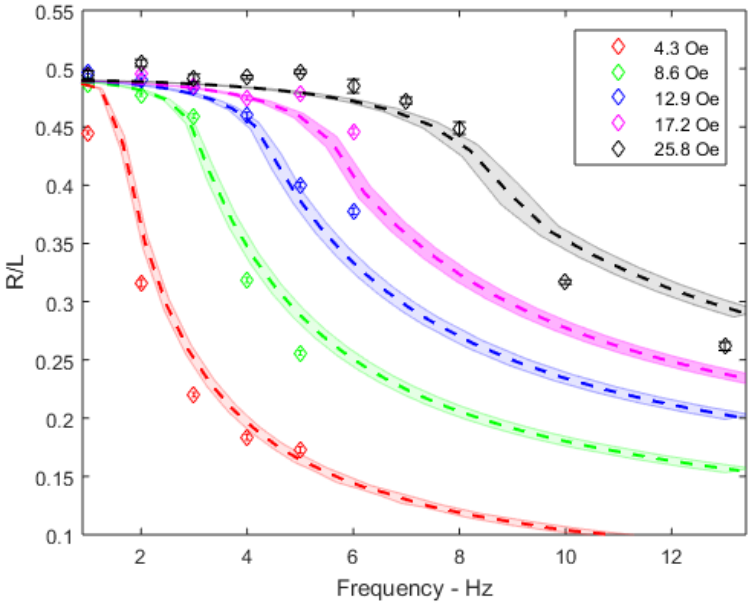

Figure 7: Filament deformation comparison between experiment and numerical results via R/L dependence on frequency. The colored diamonds denote experimental data for filament with $L = 46$ μm operating at different field strength H. The dashed lines represent numerical simulations. The shaded area represents the error margins obtained from fitting.

3 Filament dynamics under pulsed field

One important feature of ferromagnetic filaments is the instability caused when a magnetic field is inverted with respect to its magnetization, which results in either 'S' or 'U'-like filament deformation. In the latter deformation case, propulsion is experimentally observed when a pulsed magnetic field profile with a duty cycle of 30% is applied. An example of deformed filament shapes with their corresponding magnetic field direction are shown in Fig.8. The magnetic field readings in Fig.8(A) H^* are normalised by the maximum field strength value and the time t is normalised with the period of the pulsed magnetic field T. As shown in Fig.8(B)(a-c), the filament bends in a U-like shape in the 30% of the period, followed by a relaxation stage as shown Fig.8(B)(d-f). At the location shown in Fig.8(B)(f), the filament relaxes and aligns with the magnetic field direction. The swimming direction was found to be perpendicular to the magnetic field, in the y-direction. However, displacements in the x-direction were also observed, which may probably be a result of the difference in the 'arm' length of the filament, due to unequal number or sizes of the particles at each side of the 'U' shape or due to the difference in the number of DNA fragments linking particles.

The swimming behaviour is characterized by calculating the velocity perpendicular to the field direction. The centre of mass coordinate in the y-direction is first registered over time, as shown in Fig.9(a). The velocities are then estimated by a linear fit (shown as by the dashed red line in Fig.9(a)). The obtained velocities over a range of frequencies for filaments having different length L are shown in Fig.9(b), namely $L = 48$ μm (red), 59 μm (blue) and 70 μm (black). It can be shown from the obtained results in Fig.9(b), for $L = 48$ μm and 59 μm, that the velocities reach a maximum and then decrease with the increase of frequency. A maximum value of velocity was not observed for the filament with $L = 70$ μm due to the formation of a ring like shape, when the filament ends get connected.

Numerical simulations results were made using the same model presented in chapter 1, with considering the difference between perpendicular

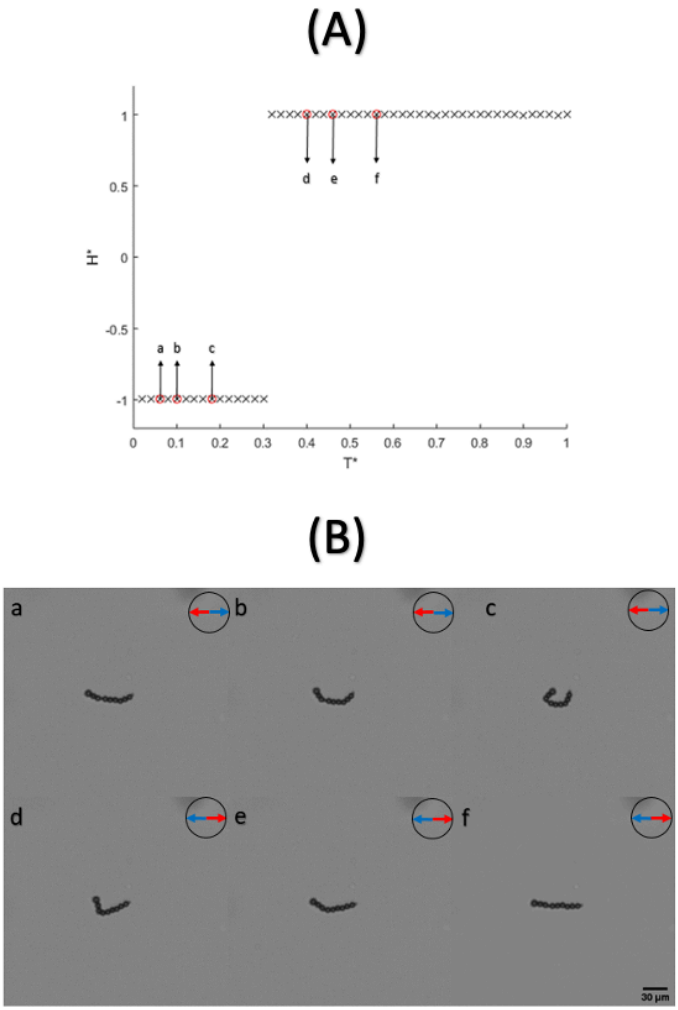

Figure 8: (A) Magnetic field measurements versus time over one period where $H^* = H/H_{\max}$ and $T^* = t/T$. The red circles show the readings that correspond to images (a-f)(B). (B) An example of filament 'U' deformations under a magnetic field with a 30% duty cycle pulse wave profile, at different location within one period for filament with length $L = 60$ μm, field frequency $f = 2$ Hz and field strength $H = 5.2$ Oe.

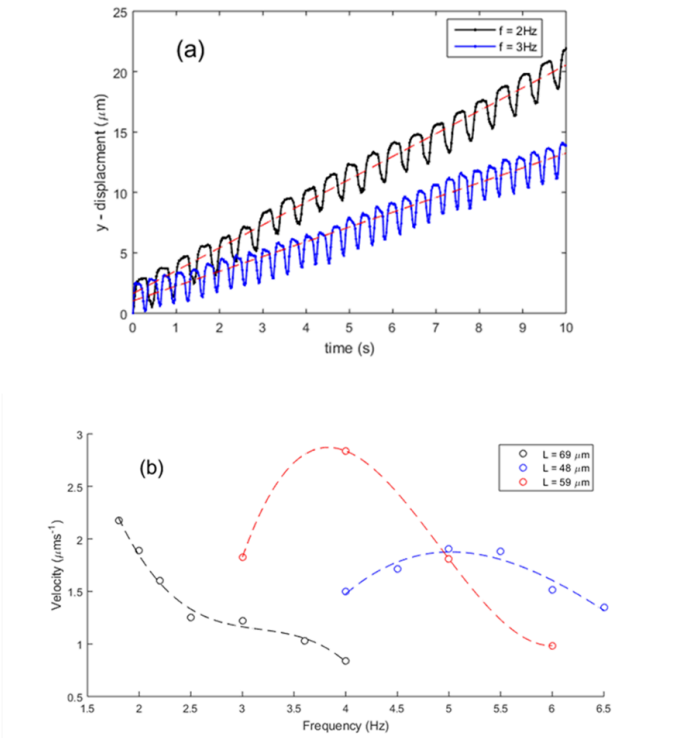

Figure 9: (a) Relationship between filament centre of mass y-displacements as a function of time for a filament with length $L = 70$ μm and frequencies $f = 2$ Hz (black line) and $f = 3$ Hz (blue line) at fixed field strength $H = 5.2$ Oe. (b) Velocity as a function of field frequency for filaments with lengths $L = 48$ μm (red), 59 μm (blue) and 70 μm (black), at a fixed field strength $H = 5.2$ Oe.

$\zeta_\perp$ and parallel $\zeta_\parallel$ hydrodynamic drag coefficients. The drag coefficient ratio is defined as λ, where λ = -($\zeta_\perp/\zeta_\parallel$ -1). Moreover, a condition is then added to the model to avoid the filament to completely relax and always have a slightly curved shape before the start of each bending stage. If the condition of initial curved shape was not applied, the 'U'-shaped deformation could not be achieved and the filament underwent the 'S'-like

deformation resulting in no propulsion. Typically a defect was observed in the chain alignment experimentally, which results in a slightly curved shape and confirms this to be a valid assumption of the added condition.

The experimentally obtained results were compared with numerical simulations, as is shown in Fig.10. In (a) of this figure, the filament center of mass y-displacements obtained experimentally, and scaled with the filament length L, are compared with numerically obtained results for three data sets - $L = 70$ μm & $f = 3$ Hz (diamonds), $L = 70$ μm & $f = 2.5$ Hz (squares) and $L = 59$ μm & $f = 3$ Hz (circles). The numerical simulations results were obtained by calculating the median obtained from the filament configurations. This corresponds to the experimentally obtained as $Cm = 70$, $T/\tau = 0.0039$ (black), $Cm = 70$, $T/\tau = 0.031$ (blue) and $Cm = 50$, $T/\tau = 0.0047$ (red) respectively. In a similar way to the experimental data processing, the velocities obtained by numerical simulation are calculated by a linear fit from the y-displacements over time relationship, and the results were compared for filaments with three different lengths, as shown in Fig.10(b). The data points for experimental velocity as shown in Fig.10(b), were previously shown in Fig.9(b), where here are scaled with L/τ on y-axis and τ on the x-axis, having filaments with length $L = 70$ μm (circle), $L = 59$ μm (square) and $L = 48$ μm (diamond). This corresponds to $Cm = 70$ (Blue), $Cm = 50$ (Black) and $Cm = 30$ (red) in numerical simulations respectively. The upper and lower limits donate the simulation results obtained by defining $\lambda = -0.4$ and $\lambda = -0.2$ respectively.

Previous studies available on the investigation of the micro-swimmer swimming behaviour have been made using chains of paramagnetic particles. For example as presented in Ido et al. 2016; Li et al. 2013; Dreyfus et al. 2005. Unlike for the chains made of paramagnetic material, where its magnetization is zero once the field is switched off, spontaneously magnetized filaments buckle when the magnetic field is inverted, in a similar way to Euler instability of a rod under the compression Pilyugina et al. 2017. This buckling instability was experimentally realized by Ērglis et al. 2010, which results in a loop formation, having the filament move in the third dimension to align with the field. Numerically, such a swimmer

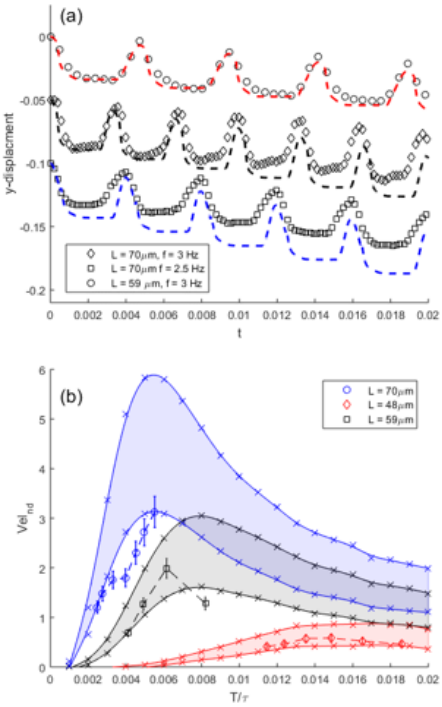

Figure 10: The filament centre of mass y-displacements as a function of time t. Circle, diamond and square points denote experimental data. The displacement is scaled by the filament length L on the y-axis and with $\tau = 54$ s (diamond and square) and 42 s (circle) on the x-axis. The dashed lines show the numerical filament centre dynamics that correspond to the experiment - $Cm = 70$, $T/\tau = 0.0039$ (black), $Cm = 70$, $T/\tau = 0.031$ (blue) and $Cm = 50$, $T/\tau = 0.0047$ (red). (b) Scatter points show velocity as a function of frequency for filaments with lengths $L = 48$ μm (diamond), 59 μm (circle) and 70 μm (square) scaled with L/τ on y-axis and τ on the x-axis, operating at a range of frequencies and fixed field strength $H = 5.2$ Oe. The solid lines represent numerical simulations over range of T/τ for $Cm = 70$ (Blue), $Cm = 50$ (Black) and $Cm = 30$ (red). Colored regions boundaries correspond to simulations by defining a slightly different $\lambda = -0.2$ and -0.4 for lower and upper lines respectively.

design was first proposed by Belovs and Cēbers 2009, showing that the filament can propel with a periodic field inversion profile, by breaking the time reversal symmetry due to the difference between bending and relaxation stages. We can compare the swimming performance through the maximum achieved velocity with other designs presented in the literature. For example, 18 $\mu m s^{-1}$, $L = 38\ \mu m, f = 30\ Hz$ were measured for a rigid helical tail swimmer with an attached magnetic bead head and driven by a rotating field profile (Zhang et al. 2009). A flexible propeller design actuated by a rotating field profile with a constant perpendicular field resulted in 21 $\mu m s^{-1}, L = 5.8\ \mu m, f = 21\ Hz$, as presented by Pak et al. 2011. The maximum velocity obtained here is $\approx 3\ \mu m s^{-1}$ which is lower than other designs of micro swimmers presented in the literature. However, the swimming velocity can be optimized by either modifying the magnetic field profile, to reduce the time for full relaxation before the bending stage. This can be seen in Fig.8(A) which corresponds to $\approx T^* = 0.67...1$.

One important aspect is choice of the duty cycle, that the filament should have enough time to develop the u-like deformations but not enough time to develop the non-linear instability of S-like shape. The choice was made based on experimental observations, in order to have more swimming filaments in the sample as a whole. Initially, when the experiments were first conducted, the duty cycle was set to 70 %, the buckling instability was found to occur in the longer part of the period. However, in that case the filament was found to eventually flip and change its magnetization direction to align with the magnetic field direction in the longer stable part of the period. Different duty cycles were tried in the experiments. For example, at 50% square profile, the filament centre part was found to orient perpendicular with the magnetic field, while the ends try to follow the magnetic field direction in the opposite direction resulting in an S-like shape in 2D and 3D motions. The cease of swimming and the transition to S-like deformations was also seen in numerical simulations by defining a sine wave inversion profile (Ērglis et al. 2011).

A good agreement is found when comparing experimental and numerical results, as presented in Fig.10(b) for velocities of filaments with three

different lengths over a range of frequencies. However, differences may arise as a result of the variation the filament physical properties, as for the bending modulus A_b due to unequal number of links between the particles or unequal section lengths. Moreover, in the numerical simulations the hydrodynamic drag coefficient ratio $\zeta_\perp / \zeta_\parallel$ was found to best fit with experimental velocities in the range of 1.2...1.4, opposite to the value of 2 for an infinite rod.

4 Local flow measurements

We present here the velocity measurement around filaments under the action of a rotating magnetic field. The measurements here are made using PIV technique, by the experimental setup discussed in section 1.3. Examples of acquired images, for a filament with length $L = 73$ μm under a rotating field of strength $H = 34.4$ Oe and $f = 1$ Hz are shown in Fig.11. The acquisition frame rate FR is set to 6 Hz, and the inter-frame time between the first and second exposure, shown in Fig.11(a) and (b) respectively, is set to 15 ms. Fig.11(a),(c)-(f) shows the first exposed frame at different location within a period.

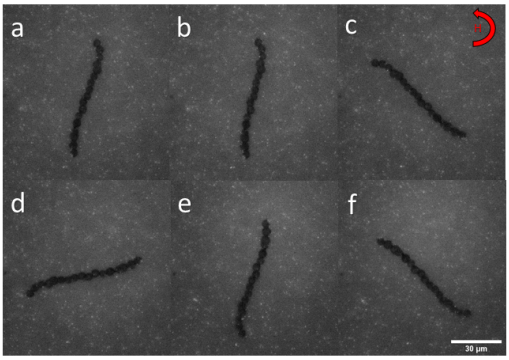

Figure 11: Examples of acquired images for local flow measurements. Filament under a rotating magnetic field of strength $H = 34.4$ Oe, frequency $f = 1$ Hz and $L = 73$ μm. (a) and (b) are the first and the second frame obtained by the double exposure mode with an inter-frame time of 15 ms. (a),(c)-(f) show the first frame acquired at different locations within one period, at a frame rate of 6 Hz.

The velocity field of the subsequent frames obtained by using the double exposure mode, at different location within the period are first obtained, using PIVlab tool. For this an add-on package for *MatLab* is used, particularly for cross-correlation calculations and PIV analysis, developed by Thielicke and Stamhuis 2014. To obtain the average velocity fields at single location (a reference frame which is chosen arbitrary, here based on the

filament tangent angle at the centre). The velocity fields are first translated based on the movements of the filament centre point, then rotated by the angle difference between the tangent at filament centre point and the reference location. The results obtained are then averaged at a reference frame, flow characteristics such as velocity magnitude and vorticity are calculated. The experiments were done for filaments of three different lengths L, under a fixed field strength $H = 34.4$ Oe and at a range of frequencies $f = 1 \rightarrow 5$ Hz. An example of the velocity fields and their magnitude normalised by the calculated velocity of a rotating rod (v_{rod}), where (v_{rod}) is the maximum calculated velocity of a rotating rod estimated theoretically, is shown in Fig.12 for a filament with $L = 73$ μm, and frequencies $f = 1 \rightarrow 5$ Hz (a-e).

As shown in Fig.12, increasing the frequency will result in the increase of the filament minor S-like deformations, and an increase of velocity magnitude. Moreover, it is observed that the maximum velocity magnitude is located near the filament tips. Slight change in the maximum velocities was found when comparing the magnitude at the filament tips, which maybe a result of unsymmetrical rotations. The flow profile obtained for the velocity magnitude v_m along the filament center line (f_L) is shown in Fig.13, for a filament with length $L = 73$ μm, $H = 34.4$ Oe and $f = 1 \rightarrow 3$ Hz for (a $\rightarrow$ c) respectively. It is found that the maximum velocities are located in the middle of the bent part of the filament close to the tip. The velocities then decrease in a linear behaviour until reaching zero at the centre of rotation. Beyond the maximum velocity towards the filament tip, the decrease of velocity was also found to be linear. This flow profile was found to have a similar behaviour at a range of frequencies, as shown in Fig.13(a-c), for a filament with an observable S-like deformation.

Far field velocities become important to consider for filament interactions with other filaments or with other solid boundaries. The far field velocities here are characterised by the spatial velocity decay as a function of distance R away from the filament. Here the y-component velocity v is read along the x-axis from the filament maximum velocity near the filament tip (x_t). The points are then fitted with $v = \frac{a}{(R-x_t)^n}$, using n =

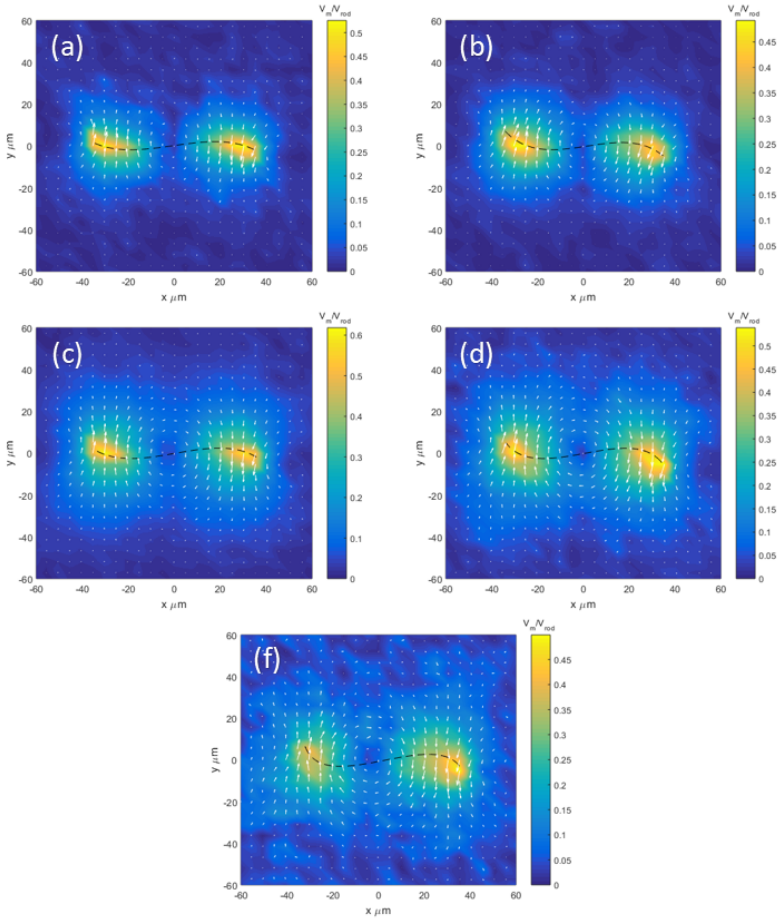

Figure 12: Velocity field obtained for a filament with length $L = 73$ μm, field strength $H = 34.4$ Oe and operating at frequency f: (a) 1 Hz, (b) 2 Hz, (c) 3 Hz, (d) 4 Hz and (e) 5 Hz

1,2,3. The results obtained for a filament with length $L = 73$ μm under a field strength $H = 34.4$ Oe are shown in Fig.14, operating at different frequencies. The results obtained show qualitatively that the best fit is obtained for a fluid velocity decay as a function of $1/R^2$, (shown as the green lines), which can be described to have a flow singularity of force

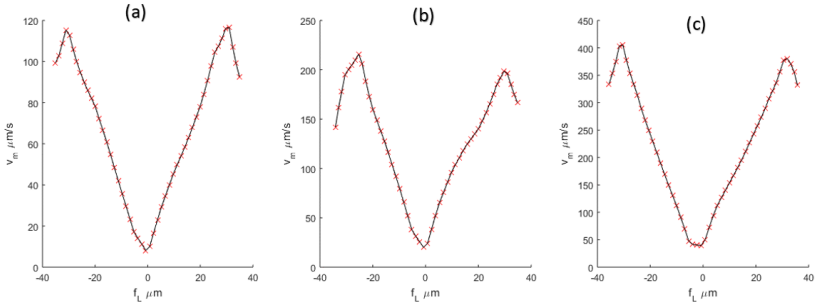

Figure 13: Flow profile of the velocity v_m along the centre line of a filament f_L with length $L = 73$ μm, frequency f: (a) = 1 Hz, (b) = 2 Hz and (c) = 3 Hz field strength $H = 34.4$ Oe

dipole.

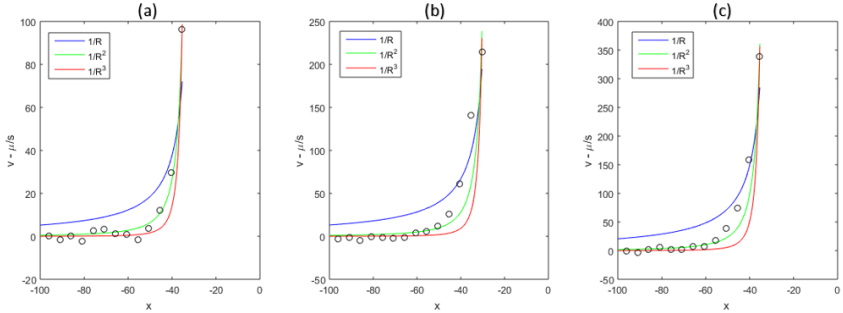

Figure 14: The fluid velocity (v) along the x-axis from the filament tip away from the filament, the black circles are read from experimental data. The lines shows the best fit obtained at different power of R, for a filament with $L = 73$ μm under a field strength $H = 34.4$ Oe and frequency for (a-c) is 1...3 Hz respectively.

Numerical simulations were done using the method of regularized Stokeslets with a regularization parameter $\delta = r/L$, defined as the ratio of particle radius to the filament length. It was found that by comparing experimental and numerical results, their behaviour are in good agreement qualitatively. However, the velocity magnitude was found to be about one order of mag-

nitude higher for numerically obtained results. A further study of the numerical method used or quantitative comparison with experimental results here is not in the scope of this work. However, further investigation can be suggested as a future work. Moreover, solving using regularized Stokeslets method introduces the regularization parameter δ, which is assumed here to be the particle diameter to filament length ratio. Simulations can be done for a wider range δ to investigate difference of flow behaviour and its applicability on this system. The difference in velocity may be explained by using higher value of δ which reduces the accuracy of results (Zhao et al. 2019). Or as a result of wall interaction that are not considered in the model.

The maximum velocity magnitude was found to be around half the expected from a rotating rigid rod, with assuming no slip condition by having the velocity at the filament boundary is equal to the fluid velocity. Here, a lower maximum measured velocities are expected compared to a rigid rod since the maximum velocities is not located at the filament tip. Moreover, the tracer particles are not located on the filament but closely around it and the fluid velocities decay as $1/R^2$, a lower maximum velocity is expected. It should be noted as observed experimentally that increasing the frequency results in rotations at larger distance from the wall bottom. It may be suggested that this effect is due to the interaction with wall.

5 Summary and conclusions

The author of this PhD thesis is trying to experimentally investigate the dynamics of chains made from ferromagnetic particles. The significance of the work presented in this thesis can be summarized in the following **conclusions**:

- It is found that under the action of rotating field ferromagnetic filaments undergo two regimes: at lower frequency the filament rotates synchronously with the rotating field and remains in its plane. At higher frequency: the filament moves out of the rotating plane in the third dimension with a circular anti-phase tip trajectory.
- It is observed under the action of periodic magnetic field inversion, the filament propels in the direction perpendicular to the field direction. However, initial filament configuration and specific field profile is required to achieve propulsion.
- Microflow measurements around filaments can be measured with a micro particle image velocimetry technique and qualitatively agree with numerical simulations.

5.1 Thesis

Results obtained justify the following **a thesis**: flexible ferromagnetic filaments can be useful for the design and development of soft microrobotics. Applications are foreseen in biomedicine and biotechnology.

References

Ahmed, Daniel, Cornel Dillinger, Ayoung Hong, and Bradley J. Nelson (2017). "Artificial Acousto-Magnetic Soft Microswimmers." In: *Advanced Materials Technologies* 2.7, p. 1700050. DOI: 10.1002/admt.201700050.

Barreto, Darius Diogo, Shashank Saxena, and Ajeet Kumar (2022). "A magnetoelastic theory for Kirchhoff rods having uniformly distributed paramagnetic inclusions and its buckling." In: *International Journal of Solids and Structures* 234-235, p. 111147. DOI: j.ijsolstr.2021.111147.

Belovs, M. and A. Cēbers (2009). "Ferromagnetic microswimmer." In: *Phys. Rev. E* 79 (5), p. 051503. DOI: 10.1103/PhysRevE.79.051503.

Biswal, Sibani Lisa and Alice P. Gast (2004). "Micromixing with Linked Chains of Paramagnetic Particles." In: *Analytical Chemistry* 76.21, pp. 6448–6455. DOI: 10.1021/ac0494580.

Brasovs, Artis, Jānis Cīmurs, Kaspars Ērglis, Andris Zeltins, Jean-Francois Berret, and Andrejs Cēbers (2015). "Magnetic microrods as a tool for microrheology." In: *Soft Matter* 11 (13), pp. 2563–2569. DOI: 10.1039/C4SM02454K.

Cēbers, Andrejs (2003). "Dynamics of a chain of magnetic particles connected with elastic linkers." In: 15.15, pp. 1335–1344. DOI: 10.1088/0953-8984/15/15/303.

Chen, Xueye and Lei Zhang (2017). "A review on micromixers actuated with magnetic nanomaterials." In: *Microchimica Acta* 184, pp. 1–11. DOI: 10.1007/s00604-017-2462-2.

Cīmurs, J. and A. Cēbers (2013). "Three-dimensional dynamics of a particle with a finite energy of magnetic anisotropy in a rotating magnetic field." In: *Physical review. E, Statistical, nonlinear, and soft matter physics* 88, p. 062315. DOI: 10.1103/PhysRevE.88.062315.

Drew, Owen, Ballard Matthew, Alexeev Alexander, and J. Hesketh Peter (2016). "Rapid microfluidic mixing via rotating magnetic microbeads." In: *Sensors and Actuators A: Physical* 251, pp. 84–91. DOI: 10.1016/j.sna.2016.09.040.

Dreyfus, Rémi, Jean Baudry, Marcus L. Roper, Marc Fermigier, Howard A. Stone, and Jérôme Bibette (2005). "Microscopic artificial swimmers." In: *Nature* 437.7060, pp. 862–865. DOI: 10.1038/nature04090.

Ērglis, K., R. Livanovičs, and A. Cēbers (2011). "Three dimensional dynamics of ferromagnetic swimmer." In: *Journal of Magnetism and Magnetic Materials* 323.10, pp. 1278–1282. DOI: 10.1016/j.jmmm.2010.11.021.

Ērglis, Kaspars (2010). "Experimental study of properties and motion of flexible magnetic microfilaments." In: *PhD Thesis, University of Latvia*. URL: https://mmml.lu.lv/publications.

Ērglis, Kaspars, Rūdolfs Livanovičs, and Andrejs Cēbers (2010). "Three dimensional instability of flexible ferromagnetic filament loop." In: *Magnetohydrodynamics* 46, pp. 245–256.

Frka-Petesic, B., K. Erglis, J.F. Berret, A. Cēbers, V. Dupuis, J. Fresnais, O. Sandre, and R. Perzynski (2011). "Dynamics of paramagnetic nanostructured rods under rotating field." In: *Journal of Magnetism and Magnetic Materials* 323.10, pp. 1309–1313. DOI: 10.1016/j.jmmm.2010.11.036.

Goubault, C., P. Jop, M. Fermigier, J. Baudry, E. Bertrand, and J. Bibette (2003). "Flexible Magnetic Filaments as Micromechanical Sensors." In: *Phys. Rev. Lett.* 91 (26), p. 260802. DOI: 10.1103/PhysRevLett.91.260802.

Ido, Yasushi, Yan-Hom Li, Hiroaki Tsutsumi, Hirotaka Sumiyoshi, and Ching-Yao Chen (2016). "Magnetic microchains and microswimmers in an oscillating magnetic field." In: *Biomicrofluidics* 10.1, p. 011902. DOI: 10.1063/1.4939945.

Koleoso, M., X. Feng, Y. Xue, Q. Li, T. Munshi, and X. Chen (2020). "Micro/Nanoscale Magnetic Robots for Biomedical Applications." In: *Materials Today Bio* 8, p. 100085. DOI: 10.1016/j.mtbio.2020.100085.

Kuei, Steve, Burke Garza, and Sibani Lisa Biswal (2017). "From strings to coils: Rotational dynamics of DNA-linked colloidal chains." In: *Phys.*

Rev. Fluids 2 (10), p. 104102. DOI: 10.1103/PhysRevFluids.2.104102.

Li, Yan-Hom, He-Ching Lin, and Ching-Yao Chen (2013). "Steering of Magnetic Micro-Swimmers." In: *IEEE Transactions on Magnetics* 49.7, pp. 4120–4123. DOI: 10.1109/TMAG.2013.2241028.

Nguyen, Kim Tien et al. (2021). "A Magnetically Guided Self-Rolled Microrobot for Targeted Drug Delivery, Real-Time X-Ray Imaging, and Microrobot Retrieval." In: *Advanced Healthcare Materials* 10.6, p. 2001681. DOI: 10.1002/adhm.202001681.

Pak, On Shun, Wei Gao, Joseph Wang, and Eric Lauga (2011). "High-speed propulsion of flexible nanowire motors: Theory and experiments." In: *Soft Matter* 7 (18), pp. 8169–8181. DOI: 10.1039/C1SM05503H.

Palkar, Vaibhav, Pavel Aprelev, Arthur Salamatin, Artis Brasovs, Olga Kuksenok, and Konstantin G. Kornev (2019). "Rotating magnetic nanorods detect minute fluctuations of magnetic field." In: *Phys. Rev. E* 100 (5), p. 051101. DOI: 10.1103/PhysRevE.100.051101.

Pilyugina, Ekaterina, Brad Krajina, Andrew J. Spakowitz, and Jay D. Schieber (2017). "Buckling a Semiflexible Polymer Chain under Compression." In: *Polymers* 9.3, p. 99. DOI: 10.3390/polym9030099.

Purcell, E. M. (1977). "Life at low Reynolds number." In: *American Journal of Physics* 45.1, pp. 3–11. DOI: 10.1119/1.10903.

Shanko, Eriola-Sophia, Yoeri van de Burgt, Patrick D. Anderson, and Jaap M. J. den Toonder (2019). "Microfluidic Magnetic Mixing at Low Reynolds Numbers and in Stagnant Fluids." In: *Micromachines* 10.11, p. 731. DOI: 10.3390/mi10110731.

Spatafora-Salazar, Aldo, Dana M. Lobmeyer, Lucas H. P. Cunha, Kedar Joshi, and Sibani Lisa Biswal (2021). "Hierarchical assemblies of superparamagnetic colloids in time-varying magnetic fields." In: *Soft Matter* 17 (5), pp. 1120–1155. DOI: 10.1039/D0SM01878C.

Taylor, G.I. (1967). "Low Reynolds Number Flows." In: *Educational Services Incorporated. Distributor: Encyclopaedia Britannica Educational Corporation, Chicago, Illinois.*

Thielicke, William and E J Stamhuis (2014). "PIVlab – Towards User-friendly, Affordable and Accurate Digital Particle Image Velocimetry in MATLAB." In: *Journal of Open Research Software* 2, e30. DOI: 10.5334/jors.bl.

Wiggins, Chris H, Daniel Riveline, Albrecht Ott, and Raymond E. Goldstein (1998). "Trapping and wiggling: elastohydrodynamics of driven microfilaments." In: *Biophysical journal* 74 2 Pt 1, pp. 1043–60. DOI: 10.1016/S0006-3495(98)74029-9.

Zhang, Li, Jake J. Abbott, Lixin Dong, Kathrin Eva Peyer, Bradley Kratochvil, Haixin Zhang, Christos Bergeles, and Bradley J. Nelson (2009). "Characterizing the swimming properties of artificial bacterial flagella." In: *Nano letters* 9 10, pp. 3663–3667. DOI: 10.1021/nl901869j.

Zhao, Boan, Eric Lauga, and Lyndon Koens (2019). "Method of regularized stokeslets: Flow analysis and improvement of convergence." In: *Phys. Rev. Fluids* 4 (8), p. 084104. DOI: 10.1103/PhysRevFluids.4.084104.